

On the inherent bias of swirling strength in defining vortical structure ^{EP}

Cite as: Phys. Fluids 31, 035107 (2019); <https://doi.org/10.1063/1.5089883>

Submitted: 23 January 2019 . Accepted: 08 March 2019 . Published Online: 27 March 2019

Peter S. Bernard 

COLLECTIONS

 This paper was selected as an Editor's Pick



[View Online](#)



[Export Citation](#)



[CrossMark](#)



CAPTURE WHAT'S POSSIBLE
WITH OUR NEW PUBLISHING ACADEMY RESOURCES

Learn more 



On the inherent bias of swirling strength in defining vortical structure

Cite as: Phys. Fluids 31, 035107 (2019); doi: 10.1063/1.5089883

Submitted: 23 January 2019 • Accepted: 8 March 2019 •

Published Online: 27 March 2019



View Online



Export Citation



CrossMark

Peter S. Bernard^{a)} 

AFFILIATIONS

Department of Mechanical Engineering, University of Maryland, College Park, Maryland 20742, USA

^{a)}Electronic mail: bernard@umd.edu.

ABSTRACT

The traditional practice of using rotational motion as the principal attribute of coherent vortical structures in the buffer region of near-wall turbulent flow is shown to create a biased accounting of the role of vorticity within the structures. Vorticity associated with rotation is given a favored consideration against vorticity that is equally strong but not associated with rotation. Using data from a highly resolved direct numerical simulation of channel flow, it is shown that describing the structures based on the properties of the rotational field leads to a distorted view of the actual structures that are present. As a practical matter, this means that where hairpins are typically considered to be the flow structures, a more accurate description of the coherent events is that they are elongated mushroom-shaped vortical objects ejecting over low speed streaks. In this, hairpin-shaped rotational regions are embedded in the lobes of the mushrooms.

Published under license by AIP Publishing. <https://doi.org/10.1063/1.5089883>

I. INTRODUCTION

Ever since the development of reliable means for locating rotational regions in turbulent flows,¹⁻³ the magnitude of the local rotation or swirling strength has become a primary means by which coherent vortical events are identified and described within transitioning and fully turbulent boundary layers. The most commonly accepted view of what the rotational regions say about structures is that they are hairpin-shaped vortices⁴⁻⁹ although plausible arguments can be made to support other interpretations of the shape of the swirling strength.¹⁰⁻¹² A well formed hairpin is viewed as being something like a vortex in the shape of a folded-over tornado. An iconic depiction of this idea is in the figure of a horseshoe vortex by Theodorsen that is widely reproduced.¹³ In fully developed turbulence, as against transition, the random flow conditions are such as to inhibit the appearance of vortices in the idealized hairpin shape so that in practice, the concept of the “hairpin vortex” is usually meant to also include hairpins deformed in various ways as well as single-legged hairpins and so forth.¹⁴

Hairpin vortices in the buffer layer within $y^+ = 100$ of a solid boundary that are associated with low-speed streaks, and which are the subject of this paper, must originate out of the intense vorticity field present in the viscous sublayer of wall-bounded flows. A

well known argument¹⁵ explains the process as involving the ejection of spanwise vorticity over low-speed streaks that is sheared forward forming into the hairpin vortices. The complete vorticity field in this dynamical process consists of the rotational region forming the hairpin and ancillary vorticity, or what we will call “supporting vorticity,” that cannot be seen via the swirling strength since it is not rotational. Such vorticity is both upstream of and coincident with locations where rotation occurs. Various aspects of the supporting vorticity can and have been visualized using vorticity lines, two-dimensional vorticity contours over streaks and three dimensional vorticity isosurfaces.¹⁶⁻²³ It is also visible as shear layers in two-dimensional (2D) velocity quiver plots where rotational patterns may sometimes^{17,24,25} (but not always^{26,27}) be attributable to hairpins.

The common assumption that the shape of the rotational field is a good indicator of the nature of the wall structure has encouraged the viewpoint that the hairpins by themselves are to be taken to be the principal vortical structures in the buffer layer. This belief is so well entrenched that current analyses of the boundary layer structure have as their goal finding and analyzing the behavior of hairpins under the implicit assumption that there is no need to inquire further as to what the structures might be. In particular, the possibility that the supporting vorticity is

sufficiently important to warrant rethinking the hairpin paradigm is not considered.

An analysis and visualization technique that has given some insight into the shape of the entire local vorticity field within structures is that based on using gridfree vortex filaments to represent the flow field. A simulation of transitional boundary layers using this methodology^{28,29} shows that the filaments organize to create structures that cannot be called hairpins, yet contain rotational regions within them that are consistent with the hairpin idea. The difference between structures in the filament calculation and hairpins is that the former contains the supporting vorticity within it as a fundamental part that cannot be reasonably set aside as unimportant to the structure itself. The overall structure in the filament calculation is best understood as being a streamwise elongated, tilted raised fold in the surface vorticity layer over low-speed streaks that develops downstream into a mushroom-like shape in which the hairpins are contained within the lobes of the mushrooms. The mushroom-like structures are similar to that seen in physical experiments wherein Göertler type vortices are generated in perturbed boundary layers^{30–32} as well as in a direct numerical simulation (DNS) of transition.³³

The supporting vorticity that occurs within and upstream of hairpins as seen in DNS studies is consistent with the behavior of the vorticity found in the structures occurring in the filament calculation. Moreover, hairpin-like rotational regions are compatible with both the hairpin model and the mushroom-like ejections seen in the filament study. These observations suggest that it is worthwhile to take a more comprehensive look at the vorticity field seen in DNS near low-speed streaks to see if the hairpins that occur there are truly self-contained structures or not. What will emerge in this study is that once the biased view that rotation is the defining element of structure is put to the side, then it is readily concluded that the standard structure along streaks consists of the ejecting vorticity that evolves into a mushroom-like form, not hairpin vortices.

II. CHANNEL FLOW SIMULATION

The DNS channel flow data used in this study were obtained from the Johns Hopkins University (JHU) turbulence database.³⁴ In this, a no-slip boundary condition is imposed on the top and bottom walls of the channel and periodic boundary conditions are applied in the longitudinal and transverse directions. The wall-normal, velocity-vorticity formulation of the Navier-Stokes equation is solved using a Fourier-Galerkin pseudo-spectral method in the longitudinal and transverse directions and a seventh-order basis-spline collocation method in the wall-normal direction. Initially, the flow is driven by a constant volume flux control. Once stationary conditions are reached, the control is changed to a mean pressure gradient forcing term. More specific simulation details including validation of the solutions have been given by the authors of Refs. 34–36.

Our analysis is for flow at Reynolds number $Re_\tau = 1000$ based on the friction velocity and channel half width. In terms of the centerline velocity, the Reynolds number is $Re_c = 22, 625$. The grid in the simulation has $2048 \times 512 \times 1536$ mesh points in the streamwise (x), wall-normal (y), and spanwise (z) directions. The scaled viscosity is $\nu = 5 \times 10^{-5}$, and the scaled mean pressure gradient

driving the flow is $d\bar{p}/dx = -0.0025$. Velocity data from the simulation are stored over the interval $0 \leq t \leq 25.9935$ in time increments of $\Delta t = 0.0013$. The size of the flow domain is $8\pi \times 2 \times 3\pi$, or in terms of wall units $25\,133 \times 2000 \times 9425$.

The JHU turbulence database provides software for extracting velocity and velocity derivative data at arbitrary points and times within the simulation. From this, the vorticity can be computed as well as, in this study, the scalar parameter λ_2 that is used for visualizing the rotation field. λ_2 is the (real) middle eigenvalue of the symmetric tensor

$$B \equiv S^2 + W^2, \quad (1)$$

where $S = (\nabla\mathbf{U} + \nabla\mathbf{U}^t)/2$ is the rate-of-strain tensor and $W = (\nabla\mathbf{U} - \nabla\mathbf{U}^t)/2$ is the rotation tensor. Regions for which $\lambda_2 < 0$ contain swirling motion,² so plotting isosurfaces of constant $\lambda_2 < 0$ gives an idea of the shape and location of such regions.

III. TWO-DIMENSIONAL VIEW OF STRUCTURES

To make clear what aspects of structures are potentially overlooked in the hairpin model, consider end-on views of a typical vortical structure that is very commonly found on slices through low-speed streaks. Figure 1 shows contours of streamwise velocity forming a mushroom-like shape in a particularly well-formed and symmetric ejection of fluid over a low speed streak. The mushroom-like shape of the U contours here is the same as one can see very clearly in DNS simulations of transition.³³ Superimposed, in thick black lines, are the contours of $\lambda_2 = -50$ that intersect this 2D plane. The rotation field is slicing through the legs of a hairpin vortex with the fluid ejection occurring between the legs. In fact, the rotation is strongly tied to the streamwise vorticity component, Ω_1 , as shown in Fig. 2, where its contours are plotted together with λ_2 . The correspondence between λ_2 and Ω_1 is very strong and fits exactly the concept that is used in defining the legs of hairpin vortices.

Now consider the corresponding distributions of the wall-normal and spanwise vorticity shown in Figs. 3 and 4, respectively. The Ω_2 field in amplitude is very much as strong as the magnitude as Ω_1 in Fig. 2 and forms in a vertical \pm pattern that may be referred to as being the “stem” of the mushroom shape formed by the low speed

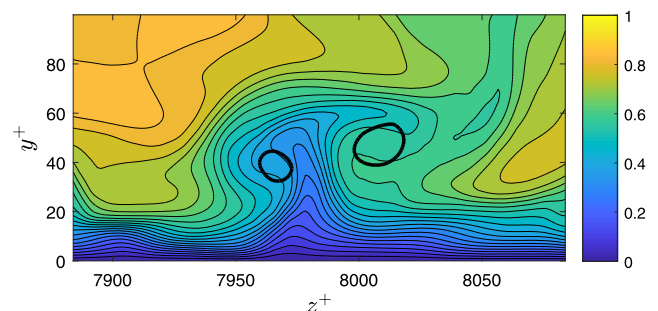


FIG. 1. Contour plot of streamwise velocity, U , at $t = 10$ from an end-on perspective centered at $x^+ = 9517$ along a low-speed streak. Intersection of $\lambda_2 = -50$ with the plane is given by heavy black lines.

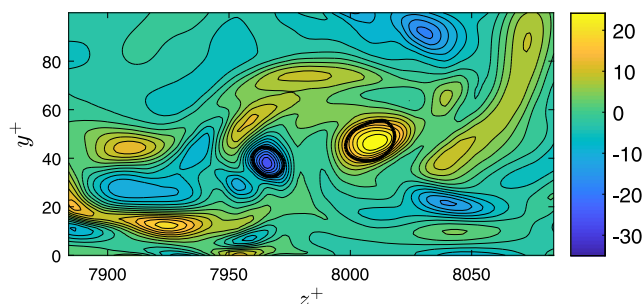


FIG. 2. Contour plot of streamwise vorticity Ω_1 and $\lambda_2 = -50$ for the same location as in Fig. 1.

ejecting fluid. Similarly, spanwise vorticity of the same overall magnitude is seen to appear over the top of the mushroom in Fig. 4. The configuration of the individual vorticity components shown in these end-on plots fits exactly the structural aspects seen in the filament calculations.

The arrangement of velocity, vorticity, and rotation in Figs. 1–4 is very common in spanwise local planes sitting over low-speed streaks. One way of demonstrating this indirectly is shown in Fig. 5 containing a contour plot of velocity contours $0 \leq U \leq 0.3$, where the local maximum velocity is $U_{max} = 1.0323$, on the plane

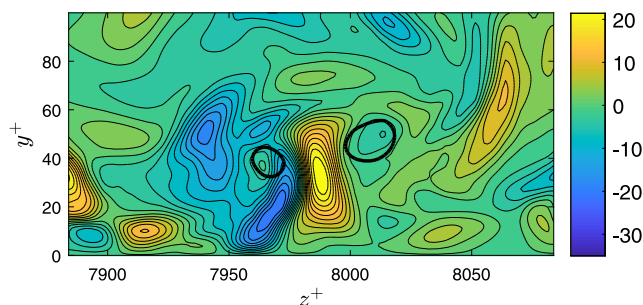


FIG. 3. Contour plot of wall-normal vorticity Ω_2 and $\lambda_2 = -50$ for the same location as in Fig. 1.

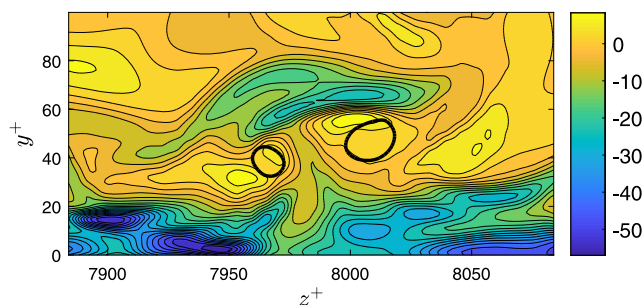


FIG. 4. Contour plot of spanwise vorticity Ω_3 and $\lambda_2 = -50$ for the same location as in Fig. 1.

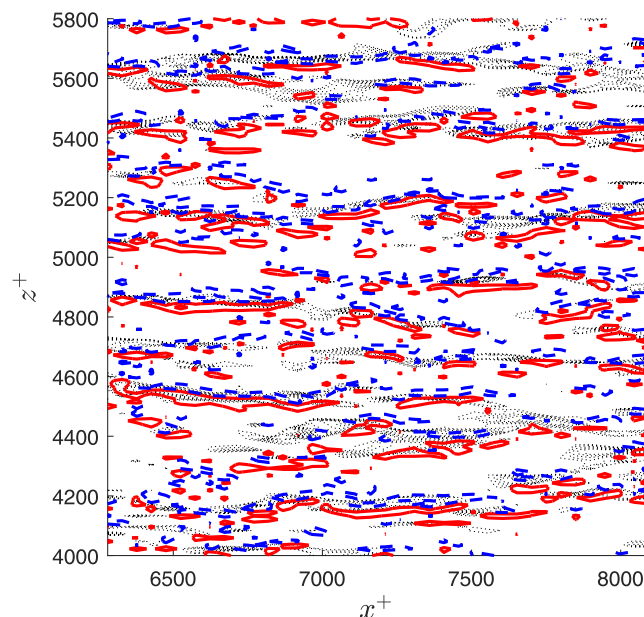


FIG. 5. Connection between wall-normal vorticity at $y^+ = 30$ and low-speed streaks at $y^+ = 10$. Red line: $\Omega_2 = 10$, blue dashed line $\Omega_2 = -10$, and black dots: streamwise velocity, $0 \leq U \leq 0.3$.

$y^+ = 10$ that marks low-speed streaks, with superimposed contours of Ω_2 taken from the plane $y^+ = 30$. The latter are seen to form numerous elongated regions of wall-normal vorticity in plus minus pairs that exactly track along the low speed regions. A similar behavior can be inferred from velocity quiver plots on planes parallel to the boundary.^{37,38} Spanwise cuts through the contours in Fig. 5 almost invariably show wall-normal vorticity contours that are similar to those seen in Fig. 3. Also visible in many of the spanwise cuts through the low-speed streaks are arrangements of streamwise and spanwise vorticity and swirling strength that are consistent with those shown in the previous example. The exact distributions of these quantities differ from one location to another due to variations in local conditions including the relative position within a structure and the distorting influence of nearby vortices. Despite these variations, for the great majority of end-on views over low-speed streaks, it is straightforward to identify the ejecting fluid, the local rotational motions that are associated with it and trends in the vorticity field that fit the example in Figs. 2–4.

IV. THREE-DIMENSIONAL VIEW OF STRUCTURES

We turn attention now to considering how the behavior of the vorticity field seen in the 2D plots is manifested in a representative three-dimensional (3D) buffer layer structure. The goal is to achieve a holistic view of how the physics of fluid ejection leading to hairpin formation occurs within entire self-contained structures. We begin with a three-dimensional view in Fig. 6 of the wall-normal vorticity field that produces the kinds of Ω_2 contours seen in Fig. 5. This particular event sits over a low-speed streak for data at $t = 15$ and

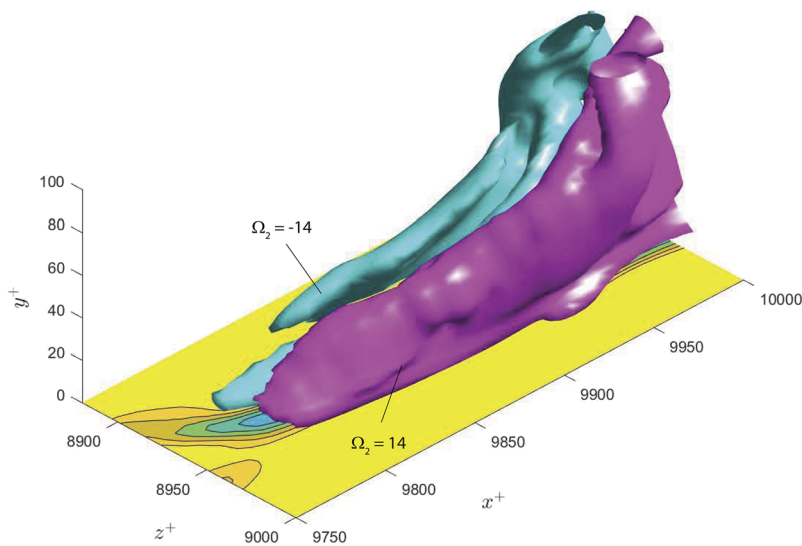


FIG. 6. Isosurfaces of wall-normal vorticity, ± 14 , as they appear in numerous events in the near-wall flow. Contour plot of $0 \leq U \leq 0.4$ in the ground plane.

is approximately 200 wall units in the streamwise extent. The wall-normal vorticity is seen to form a \pm pattern to either side of the streak that rises upward reaching to $y^+ = 100$ at the downstream end. The growing height of the Ω_2 field with downstream distance fits in with the idea of the spanwise vorticity rising up over low speed streaks to form the stems of the mushroom-like vorticity field within which the hairpins are embedded.

The source of Ω_2 in Fig. 6 is expected to lie in the reorientation of spanwise vorticity as it is ejected outward. Such a rise in the spanwise vorticity field over low speed streaks has been observed in streamwise 2D contour plots.²⁰ A view of the same phenomenon as 3D isosurfaces of the Ω_3 field is shown in Fig. 7 that corresponds to the structure in Fig. 6. In particular, it is seen that the Ω_3 surface rises upward in coordination with that of the Ω_2 field. The close relationship between Ω_2 and Ω_3 is illustrated by their seamless

connection in the image in Fig. 8 where the isosurfaces in Figs. 6 and 7 are plotted together. The abrupt downstream end to Ω_3 seen in the figures indicates the limits of the ejection as well as the end result of the reorientation of spanwise vorticity.

At the upstream end of the vorticity surfaces shown in Figs. 6–8, spanwise vorticity rises a small amount and with it \pm wall-normal vorticity develops. At the same time, the presence of shearing begins the process of creating streamwise vorticity that starts near the wall and rises upwards through the structure eventually forming the hairpin shape. Some idea of how the roll-up into the hairpin legs develops can be seen by following tracer particles.²⁹ The mechanism involves the presence of points in the flow where slow moving ejecting fluid meets high speed fluid arcing in from the sides leading to a consequent reorientation of the wall-normal and spanwise vorticity into the streamwise direction. Such streamwise vorticity produced

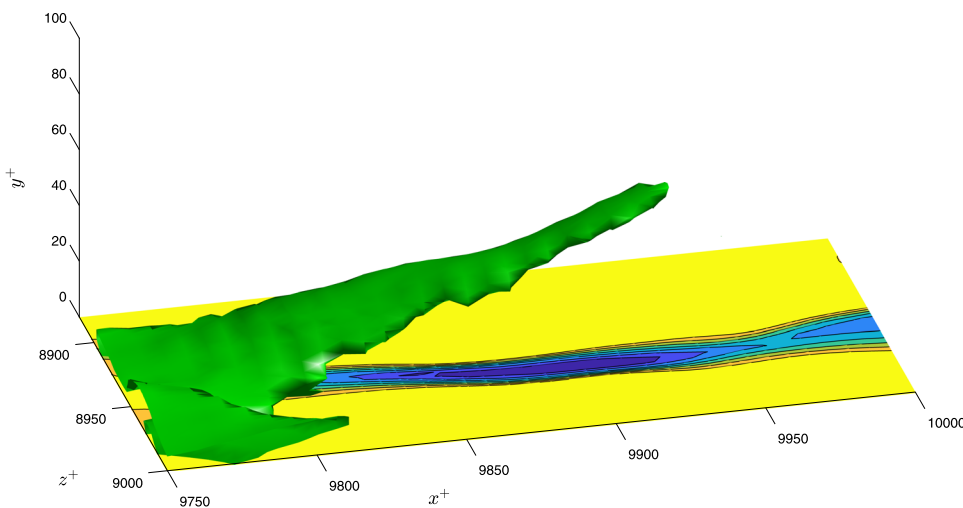


FIG. 7. Isosurface of $\Omega_3 = -25$ corresponding to the same event depicted in Fig. 6. The accompanying streamwise velocity for $0 \leq U \leq 0.4$ is shown in the ground plane. The raised Ω_3 surface is directly over the low speed streak.

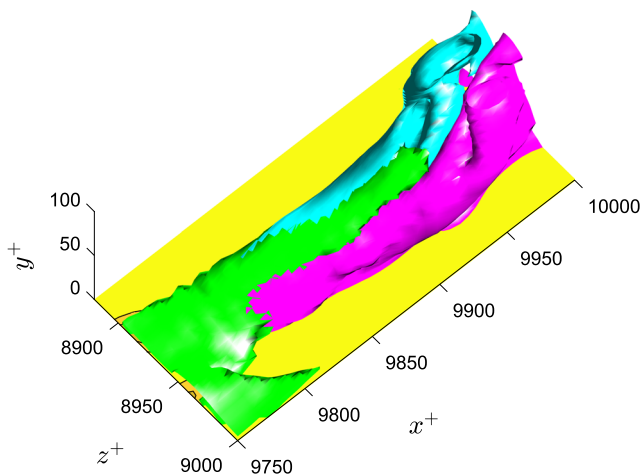


FIG. 8. The isosurfaces of Ω_2 and Ω_3 contained in Figs. 6 and 7 brought together into one plot.

by this process is shown in Fig. 9 containing a plot of the Ω_1 isosurfaces with the values ± 14 . The streamwise vorticity field has all the expected attributes of a hairpin and, according to Figs. 6 and 9, sits at the highest part of the stem region formed by Ω_2 . Ω_1 and Ω_2 overlap where the orientation of the total vorticity is tilted at an angle with respect to the streamwise direction. An important point is that the wall-normal vorticity fills the region underneath the hairpin forming the stem part of the mushroom-like ejection of vorticity.

The isosurfaces of the three vorticity components that have been mapped out in Figs. 6–9 for one particular event point to the presence of a structure that is similar to that seen in the filament calculations of transition. This includes lift up of spanwise vorticity leading to the \pm isosurfaces of Ω_2 that grow with downstream distance and out of which the hairpin shaped Ω_1 field appears. It is not surprising then to see that the rotational region for this structure, shown in Fig. 10, forms a hairpin that coincides with the shape of

the Ω_1 field. As was emphasized in the 2D views, the magnitude of Ω_1 within the hairpin is not different than the magnitudes of the Ω_2 and Ω_3 fields that compose supporting parts of the overall structure. It is not evident why the subjective isolation of the hairpin region due to its rotational properties is suitable justification for calling this a structure in its own right. The vortical structure that is present in the flow here, viewed as an entire entity, is the raised fold in the surface vorticity that culminates in the mushroom-like vorticity field containing a hairpin.

The type of event illustrated in Figs. 6–10 is found to be commonplace along low-speed streaks in the simulation. This fits in with the fact that 2D views similar to those shown previously occur widely in the flow and the suggestion in Fig. 5 that the trend in Ω_2 occurring along streaks is ubiquitous throughout the flow field. Some indication of the frequency of occurrence of the vortical events may be gleaned from Figs. 11 and 12 showing the Ω_2 and Ω_3 fields along a typical low-speed streak in the simulation. Here, there is a sequence of four events wherein the spanwise vorticity is rising above the streak, with the wall-normal vorticity aligned as in Fig. 6. Each of these four events can be expected to culminate in the formation of streamwise vorticity associated with a mushroom-like shape containing hairpin-shaped rotation.

The rotation field corresponding to the events in Figs. 11 and 12 is shown in Fig. 13 where an attempt has been made to link specific rotational regions to specific events. The identification scheme used here is based on examining simultaneous plots of the Ω_2 field in Fig. 11 with that of λ_2 in order to see where the latter has emerged from the former. It is evident that, apart from the first of the four structures where a somewhat clearly identifiable hairpin is present, the rotation fields produced by the other ejection events fall into the category of deformed hairpins and may be easily overlooked in taking an inventory of events near the boundary in the simulation.

The difficulties in finding hairpins via swirling strength as in Fig. 13 are common to any turbulent flow simulation. In practice, there is generally a wide latitude in the way that hairpins are selected out of the visible rotational regions. In some cases, events as well-organized as that in Fig. 10 are selected.⁹ In others, arch vortices are taken to be hairpins,²⁴ and in others, the requirement for being

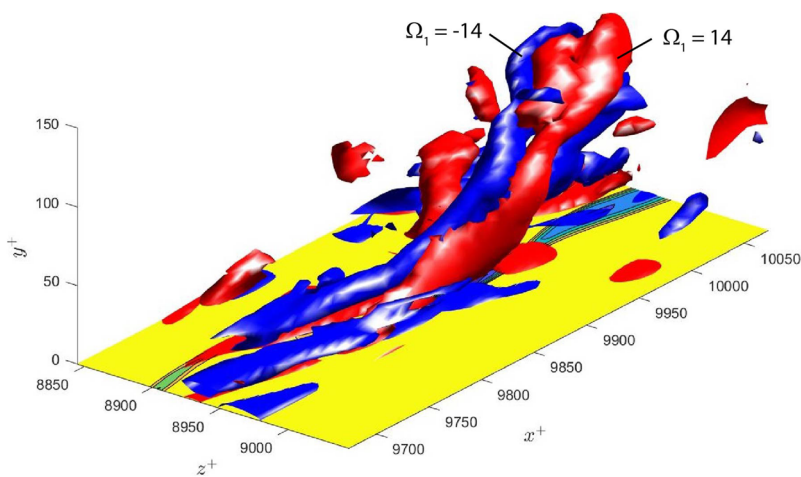


FIG. 9. Isosurfaces of $\Omega_1 = \pm 14$ for the event in Fig. 6.

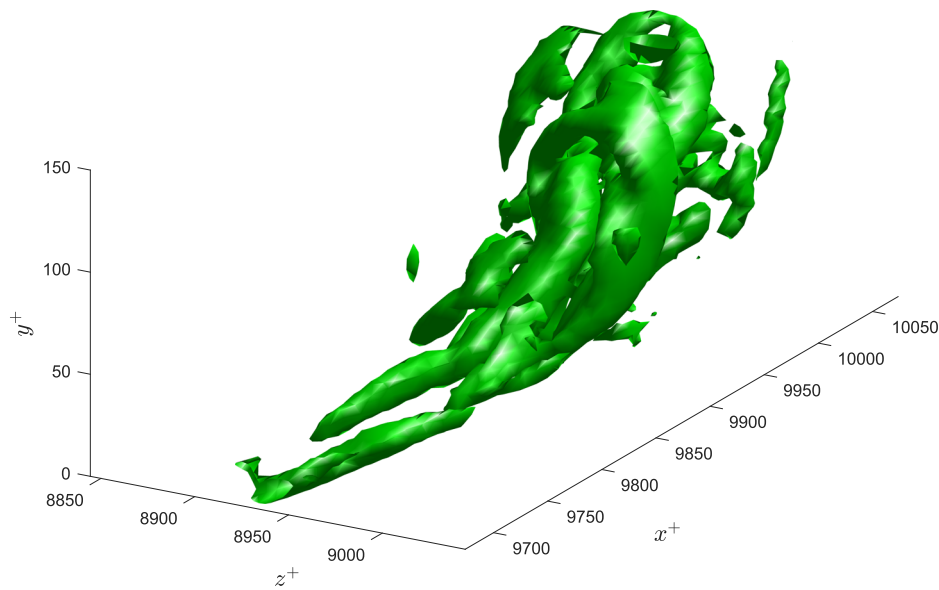


FIG. 10. Isosurfaces of $\lambda_2 = -20$ for the event in Fig. 6.

a hairpin is merely the presence of streamwise rotational motion.²¹ It should be clear from the present analysis that visualizations of Ω_2 and Ω_3 that are the upstream precursors to the hairpins have a considerably less chaotic and more repeatable pattern than does the rotation field spawned from them. Thus, beside their essential role as part of the vortical structures, there is clearly value in visualizing the

entire vorticity field along streaks in the search for coherent vortices in the buffer layer.

The relative lack of organization in the hairpins, as against the Ω_2 and Ω_3 fields, is likely due to them being the last part of the structures to fully emerge as well as the fact that they are furthest from the wall. For both reasons, they are likely to be more influenced

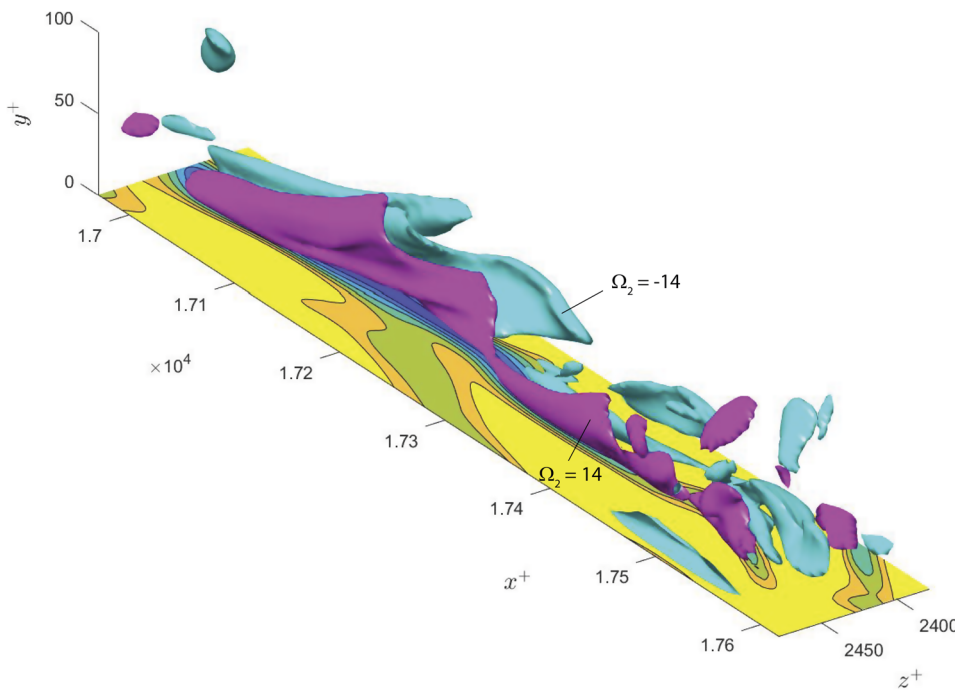


FIG. 11. Wall-normal vorticity signatures of four hairpins along a single, low-speed streak at $t = 10$. Contour plot of $0 \leq U \leq 0.4$ in the ground plane.

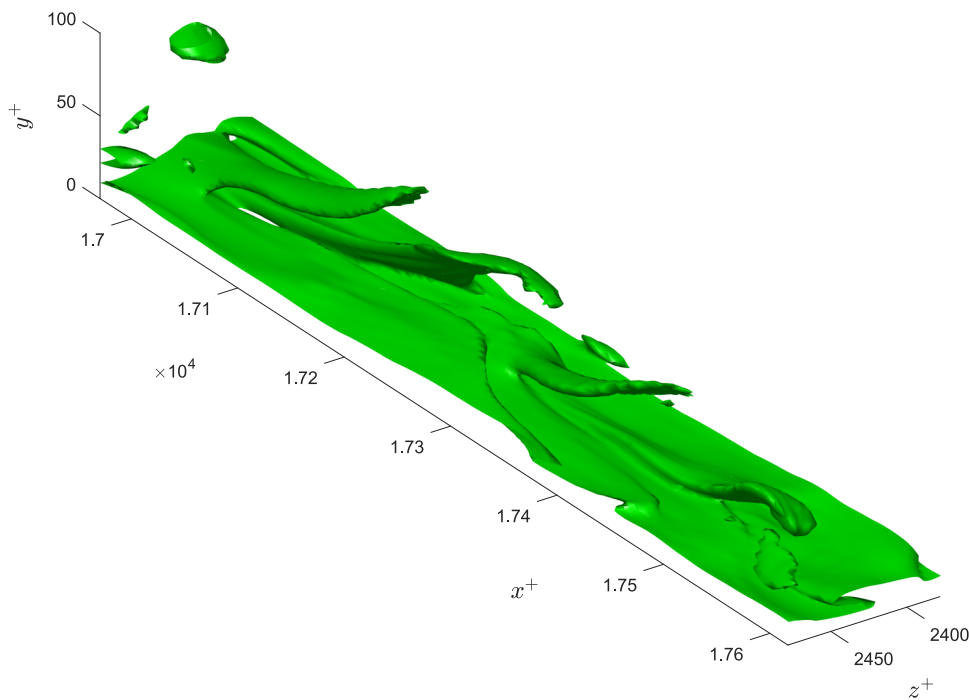


FIG. 12. Spanwise vorticity isosurfaces $\Omega_3 = -18$ corresponding to the same events as in Fig. 11.

by the fundamental randomness of the flow field, than the emerging and ejecting vorticity that creates a pattern in Ω_2 and Ω_3 . Other nearby vortices have a greater opportunity to influence the shape of the developing structure as it ejects further from the wall over an extended time period. In order for the nascent hairpins to maintain

the shapes that are commonly seen in transition requires the relative absence of nearby distorting structures. The presence of events such as that in Fig. 10 testifies to the fact that such conditions, more or less, do occur from time to time and from place to place in the fully turbulent region.

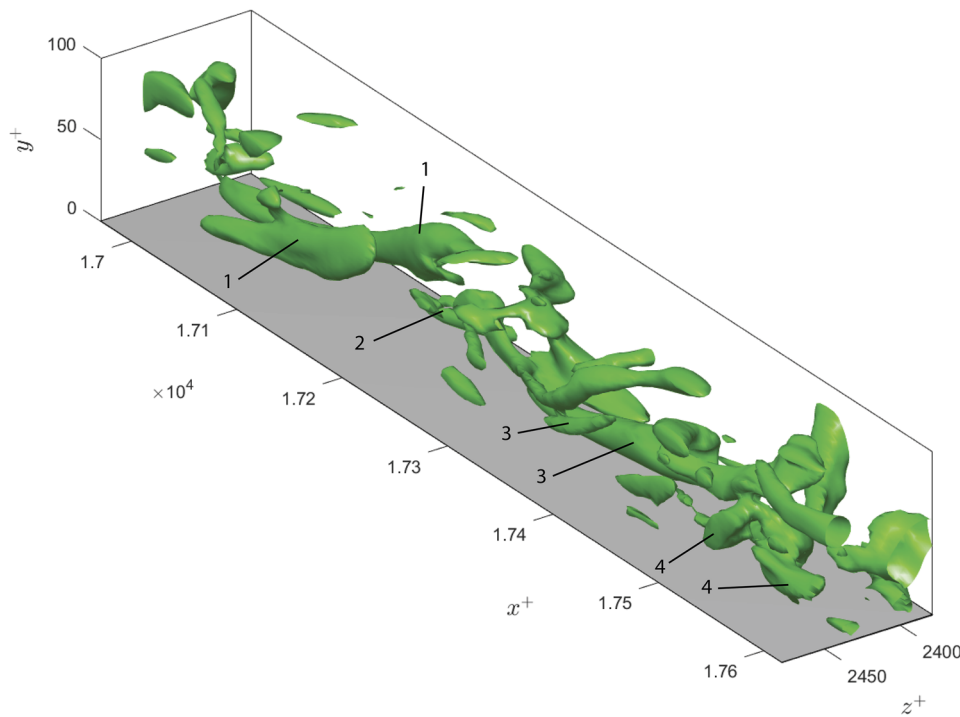


FIG. 13. Isosurfaces of $\lambda_2 = -25$ for the same sequence of events as in Fig. 11.

The repeatable patterns in Ω_2 and Ω_3 that are associated with hairpin development can also be used to advantage in tracing the dynamics of the flow field that produces hairpin-like rotational regions. Thus, while the vorticity field satisfies a conservation law that allows the dynamics of vorticity to be understood, the rotational motion obeys no such law so that its identification and evolution in the flow is almost entirely an exercise in subjectivity. For example, thresholds have to be set that define the size and shape of the hairpin and these must change in time in order to trace their prior history. Similarly, the connection between individual hairpins that may form groups known as packets⁴ requires the arbitrary identification of a series of rotational regions. By contrast, the vorticity field can be used to objectively tie together multiple structures and follow their mutual dynamics.

V. CONCLUSIONS

It has been shown that a consequence of defining the turbulent structure according to the magnitude of the swirling strength is that an inherent bias is created in what kinds of structures can be found. Strong non-rotational effects of the same magnitude of the rotation field are routinely set aside as being of secondary importance because of the focus on rotation. If all vorticity in a structure is judged to be equally important in defining the structure, then it is seen through the examples taken from DNS data in the buffer layer of a channel flow that ejecting spanwise vorticity leading to a mushroom-like shape is the predominant coherent structure in the flow. Hairpin-shaped regions develop within the mushroom-like structures but do not well characterize the actual objects in the flow field.

An important advantage in using the entire vorticity field in defining the structure is that this leads to a means of understanding the dynamics and history of structure that is not possible from the swirling strength. In particular, relatively clearly observable patterns in the wall-normal and spanwise vorticities sitting over low-speed streaks provide an unambiguous entry into locating and tracking the development of coherent vortical events that would otherwise be difficult or impossible to study from the rotation field. The swirling strength is seen to be more susceptible to the distorting effects of the random flow field than the non-rotational parts of the vorticity, presumably due to its position at the end-development of the structures.

Note added in proof. The MATLAB codes used in producing the figures in this paper from the data at JHU are available from the author upon request.

ACKNOWLEDGMENTS

This study was supported by the U.S. Army under Contract No. W911NF-16-2-0143. The numerical data used for this study were obtained from the Johns Hopkins Turbulence Database (JHTDB) at <http://turbulence.pha.jhu.edu>.

REFERENCES

- M. S. Chong, A. E. Perry, and B. J. Cantwell, "A general classification of three-dimensional flow fields," *Phys. Fluids A* **2**, 765–777 (1990).
- J. Jeong, F. Hussain, F. Schoppa, and J. Kim, "Coherent structures near the wall in a turbulent channel flow," *J. Fluid Mech.* **332**, 185–214 (1997).
- P. Chakraborty, S. Balachandar, and R. J. Adrian, "On the relationship between local vortex identification schemes," *J. Fluid Mech.* **535**, 189–214 (2005).
- R. J. Adrian, "Hairpin vortex organization in wall turbulence," *Phys. Fluids* **19**, 041301 (2007).
- I. Marusic, B. J. McKeon, P. A. Monkewitz, H. M. Nagib, A. J. Smits, and K. R. Sreenivasan, "Wall-bounded turbulent flows at high Reynolds numbers: Recent advances and key issues," *Phys. Fluids* **22**, 065103 (2010).
- G. E. Elsinga, R. J. Adrian, B. W. van Oudheusden, and F. Scarano, "Three-dimensional vortex organization in a high-Reynolds-number supersonic turbulent boundary layer," *J. Fluid Mech.* **644**, 35–60 (2010).
- A. J. Smits, B. J. McKeon, and I. Marusic, "High-Reynolds number wall turbulence," *Annu. Rev. Fluid Mech.* **43**, 353–375 (2011).
- D. J. C. Dennis and T. B. Nickels, "Experimental measurement of large-scale three-dimensional structures in a turbulent boundary layer. Part 1. Vortex packets," *J. Fluid Mech.* **673**, 180–217 (2011).
- Y. Jodai and G. E. Elsinga, "Experimental observation of hairpin auto-generation events in a turbulent boundary layer," *J. Fluid Mech.* **795**, 611–633 (2016).
- J. C. del Álamo, J. Jiménez, P. Zandonade, and R. D. Moser, "Self-similar vortex clusters in the turbulent logarithmic region," *J. Fluid Mech.* **561**, 329–358 (2006).
- C. Liu, L. Chen, P. Lu, and X. Liu, "Study on multiple ring-like vortex formation and small vortex generation in late flow transition on a flat plate," *Theor. Comput. Fluid Dyn.* **27**, 41–70 (2013).
- P. Schlatter, Q. Li, R. Orlu, F. Hussain, and D. S. Henningson, "On the near-wall vortical structures at moderate Reynolds numbers," *Eur. J. Mech. B: Fluids* **48**, 75–93 (2014).
- T. Theodorsen, "Mechanism of turbulence," in Proceedings of the Midwestern Conference on Fluid Mechanics, 1952.
- K. Kim, H. J. Sung, and R. J. Adrian, "Effects of background noise on generating coherent packets of hairpin vortices," *Phys. Fluids* **20**, 105107 (2008).
- S. Robinson, "Coherent motions in the turbulent boundary layer," *Annu. Rev. Fluid Mech.* **23**, 601–639 (1991).
- U. Rist and H. Fasel, "Direct numerical simulation of controlled transition in a flat-plate boundary layer," *J. Fluid Mech.* **298**, 211–248 (1995).
- J. Zhou, R. J. Adrian, S. Balachandar, and T. M. Kendall, "Mechanisms for generating coherent packets of hairpin vortices in channel flow," *J. Fluid Mech.* **387**, 353–396 (1999).
- S. Bake, D. G. W. Meyer, and U. Rist, "Turbulence mechanism in Klebanoff transition: A quantitative comparison of experiment and direct numerical simulation," *J. Fluid Mech.* **459**, 217–243 (2002).
- A. Helgeland, B. A. P. Reif, O. Andraessen, and C. E. Wasberg, "Visualization of vorticity and vortices in wall-bounded turbulent flows," *IEEE Trans. Visualization Comput. Graphics* **13**, 1055–1066 (2007).
- M. J. Ringuette, M. Wu, and M. P. Martin, "Coherent structures in direct numerical simulation of turbulent boundary layers at Mach 3," *J. Fluid Mech.* **594**, 59–69 (2008).
- J. Sheng, E. Malkiel, and J. Katz, "Buffer layer structures associated with extreme wall stress events in a smooth wall turbulent boundary layer," *J. Fluid Mech.* **633**, 17–60 (2009).
- J. M. Wallace, G. I. Park, X. Wu, and P. Moin, "Mechanism of turbulence," in Proceedings of the Summer Program, 2010.
- G. Eitel-Amor, O. Flores, and P. Schlatter, "Hairpin vortices in turbulent boundary layers," *J. Phys.: Conf. Ser.* **506**, 012008 (2014).
- R. J. Adrian and Z. C. Liu, "Observation of vortex packets in direct numerical simulation of fully turbulent channel flow," *J. Visualization* **5**, 9–19 (2002).
- W. T. Hambleton, N. Hutchins, and I. Marusic, "Simultaneous orthogonal-plane particle image velocimetry measurements in a turbulent boundary layer," *J. Fluid Mech.* **560**, 53–64 (2006).
- S. Rahgozar and Y. Maciel, "A visual assessment of hairpin packet structures in a DNS of a turbulent boundary layer," *Eur. J. Mech. B: Fluids* **56**, 161–171 (2016).
- J. Soria, V. Kitsios, and C. Atkinson, "On the identification of intense Reynolds stress structures in wall-bounded flows using information-limited two-dimensional planar data," *Eur. J. Mech. B: Fluids* **55**, 279–285 (2016).

- ²⁸P. S. Bernard, “The hairpin vortex illusion,” *J. Phys.: Conf. Ser.* **318**, 060024 (2011).
- ²⁹P. S. Bernard, “Vortex dynamics in transitional and turbulent boundary layers,” *AIAA J.* **51**, 1828–1842 (2013).
- ³⁰H. Mitsudharmadi, S. H. Winoto, and D. A. Shah, “Development of most amplified wavelength Görtler vortices,” *Phys. Fluids* **18**, 014101 (2006).
- ³¹A. C. Budiman, H. Mitsudharmadi, Y. Bouremel, S. H. Winoto, and H. T. Low, “Visualization of pre-set vortices in boundary layer flow over wavy surface in rectangular channel,” *J. Visualization* **18**, 669–677 (2015).
- ³²S. H. Winoto, H. Mitsudharmadi, A. C. Budiman, S. M. Hasheminejad, T. Nadesan, Tandiono, H. T. Low, and T. S. Lee, “On generating counter-rotating streamwise vortices,” *IOP Conf. Ser.: Mater. Sci. Eng.* **88**, 012001 (2015).
- ³³M. Buffat, L. L. Penven, A. Cadiou, and J. Montagnier, “DNS of bypass transition in entrance channel flow induced by boundary layer interaction,” *Eur. J. Mech. B: Fluids* **43**, 1–13 (2014).
- ³⁴Y. Li, E. Perlman, M. Wan, Y. Yang, C. Meneveau, R. Burns, S. Chen, A. Szalay, and G. Eyink, “A public turbulence database cluster and applications to study Lagrangian evolution of velocity increments in turbulence,” *J. Turbul.* **9**, N31 (2008).
- ³⁵J. Graham, K. Kanov, X. I. A. Yang, M. Lee, N. Malaya, C. C. Lalescu, R. Burns, G. Eyink, A. Szalay, R. D. Moser, and C. Meneveau, “A web services accessible database of turbulent channel flow and its use for testing a new integral wall model for LES,” *J. Turbul.* **17**, 181–215 (2016).
- ³⁶E. Perlman, R. Burns, Y. Li, and C. Meneveau, “Data exploration of turbulence simulations using a database cluster,” in *Proceedings of the 2007 ACM/IEEE Conference on Supercomputing* (IEEE, 2007), pp. 1–11.
- ³⁷B. Ganapathisubramani, E. K. Longmire, and I. Marusic, “Characteristics of vortex packets in turbulent boundary layers,” *J. Fluid Mech.* **478**, 35–46 (2003).
- ³⁸C. D. Tomkins and R. J. Adrian, “Spanwise structure and scale growth in turbulent boundary layers,” *J. Fluid Mech.* **490**, 37–74 (2003).